

# Mechanical Analysis of Atherosclerotic Plaques Based on Optical Coherence Tomography

ALEXANDRA H. CHAU,<sup>1,2</sup> RAYMOND C. CHAN,<sup>2</sup> MILEN SHISHKOV,<sup>2</sup> BRIAIN MACNEILL,<sup>2</sup> NICUSOR IFTIMIA,<sup>2</sup> GUILLERMO J. TEARNEY,<sup>2</sup> ROGER D. KAMM,<sup>1</sup> BRETT E. BOUMA,<sup>2</sup> and MOHAMMAD R. KAAZEMPUR-MOFRAD<sup>1</sup>

<sup>1</sup>Department of Mechanical Engineering and Biological Engineering Division, Massachusetts Institute of Technology, Cambridge, MA 02139 and <sup>2</sup>Wellman Center for Photomedicine, Massachusetts General Hospital, Harvard Medical School, Boston, MA 02114

(Received 16 January 2004; accepted 20 July 2004)

**Abstract**—Finite element analysis is a powerful tool for investigating the biomechanics of atherosclerosis and has thereby provided an improved understanding of acute myocardial infarction. Structural analysis of arterial walls is traditionally performed using geometry contours derived from histology. In this paper we demonstrate the first use of a new imaging technique, optical coherence tomography (OCT), as a basis for finite element analysis. There are two primary benefits of OCT relative to histology: 1) imaging is performed without excessive tissue handling, providing a more realistic geometry than histology and avoiding structural artifacts common to histologic processing, and 2) OCT imaging can be performed *in vivo*, making it possible to study disease progression and the effect of therapeutic treatments in animal models and living patients. Patterns of mechanical stress and strain distributions computed from finite element analysis based on OCT were compared with those from modeling based on “gold standard” histology. Our results indicate that vascular structure and composition determined by OCT provides an adequate basis for investigating the biomechanical factors relevant to atherosclerosis and acute myocardial infarction.

**Keywords**—Optical coherence tomography (OCT), FEM, Atherosclerotic plaques.

## INTRODUCTION

Acute myocardial infarction (AMI) is the leading cause of death in the United States and industrialized countries.<sup>1,2</sup> Research conducted over the past 15 years has demonstrated that specific minimally or modestly stenotic atherosclerotic plaques, termed vulnerable plaques, are precursors to coronary thrombosis, myocardial ischemia, and sudden cardiac death. Postmortem studies have identified one type of vulnerable plaque, the thin-cap fibroatheroma (TCFA), as the culprit lesion in approximately 80% of sudden cardiac deaths.<sup>7,11,20</sup> The TCFA is typically a minimally occlu-

sive plaque characterized histologically by the following features: 1) thin fibrous cap ( $<65 \mu\text{m}$ ), 2) large lipid pool, and 3) activated macrophages near the fibrous cap. Finite element analyses of vessel models derived from histology have suggested that a thin, structurally compromised fibrous cap may result in elevated focal stress and be susceptible to disruption.<sup>6,21</sup> Following rupture, the release of procoagulation factors, such as tissue factor, create a nidus for thrombus formation and the potential for an acute coronary event.<sup>37</sup>

Investigation of the biomechanics of atherosclerosis has relied upon finite element analysis for computing stress and strain distributions in idealized vascular cross-sections<sup>18,29</sup> or more realistic morphology derived from histology of autopsy specimens.<sup>12,23,25</sup> While these studies have provided important insight into disease progression and acute events, several pressing questions remain that cannot be addressed with a retrospective, *ex vivo* methodology. In addition, a nondestructive means for determining vascular structure and composition would facilitate the investigation of biomechanical response to new interventional strategies.

The current “gold standard” for determining plaque geometry and composition is histology. Although histology provides excellent resolution and, through the application of tissue-specific stains, can provide clear delineation of tissue composition, histology processing is known to cause geometry artifacts. During processing, nonuniform tissue shrinkage can give rise to distortion and warping of vascular geometry. Additionally, since histology processing requires manipulation of tissue sections as thin as  $5\text{--}10 \mu\text{m}$ , further warping, folding, and tearing of the tissue section is common. These artifacts are difficult to characterize and limit the accuracy of geometric models for biomechanical analyses.

A more attractive approach would be to base model construction on a noninvasive imaging modality. Although angiography is routinely used for detecting coronary stenoses and for directing intravascular intervention, it is limited

---

Address correspondence to Dr. Mohammad Kaazempur-Mofrad, 77 Massachusetts Avenue, Room NE47-317, Cambridge, MA 02139. Electronic mail: mrk@mit.edu

to the visualization of the vascular lumen and does not provide information regarding the structure of the vessel wall. Magnetic resonance (MR) and computed tomography (CT) imaging have been increasingly used for evaluating vascular structure but lack sufficient resolution ( $\sim 500 \times 1000 \mu\text{m}$  for *in vivo* MR,<sup>5</sup>  $\sim 600 \times 600 \mu\text{m}$  for CT<sup>4</sup>) for construction of detailed finite element models which incorporate local variations in plaque composition. Intravascular ultrasound (IVUS) is used routinely for assessing vascular structure and stent deployment but is limited to a resolution of  $\sim 100 \mu\text{m}$  and provides limited contrast between typical plaque tissue components. An IVUS based model was developed to predict rupture during *in vitro* balloon angioplasty.<sup>22</sup> IVUS images of 16 coronary specimens were digitized and outlined to create the structural models. An angioplasty balloon was inserted in each specimen and inflated until rupture occurred. Histologic confirmation of rupture location showed that 17 of 18 fractures occurred in segments having high stress and 82% of these fractures occurred at locations of high stress. No correlation was found, however, between predicted peak stress and balloon pressure at fracture. The lack of correlation was attributed to the low resolution of IVUS and its inability to detect local variations in material composition.

Optical coherence tomography (OCT) is a recently developed optical analog of IVUS that provides high-resolution ( $10 \times 25 \mu\text{m}$ ) cross-sectional images of human tissue.<sup>13,32</sup> Studies conducted *ex vivo* have demonstrated that this new imaging modality is capable of accurately characterizing the structure and composition of normal vessels and atherosclerotic plaques.<sup>33,34,36</sup> OCT catheters, suitable for intravascular application, have recently been developed and applied for imaging coronary arteries in patients. *In vivo* OCT imaging is facilitated by an 8–10 cc saline flush to allow clear visualization of the vessel wall.<sup>16</sup> Potential applications of OCT-based finite element modeling include patient-specific modeling and diagnosis and studies of disease progression and treatment efficacy. With its ability to provide high-resolution images of plaque structure *in vivo*, OCT is ideally suited for investigating plaque biomechanics using finite element modeling. However, the major drawback of OCT as a basis for modeling is the limited depth penetration inherent to the modality, which is often not sufficient to visualize through the entire thickness of the vessel wall. Thus, ambiguities in external structure identification can result, which can compromise the accuracy of the finite element analysis.

In this study, we determine the geometry of excised human coronary vessels using both OCT imaging and the conventional histology method. Using these geometries, we construct finite element models and then compare stress and strain distributions in order to assess the feasibility of OCT as a basis for finite element analysis. Finally, we

investigate the effect of OCT's limited depth penetration and subsequent outer contour ambiguity by examining the sensitivity of stress and strain distributions to perturbations in outer contour geometry.

## METHODS

### *OCT Imaging*

Optical coherence tomography (OCT) is the optical analog to time-of-flight B-mode ultrasound. A beam of near infrared light is sent into the sample and the light scattering properties of the tissue are interrogated. Because of the far shorter optical wavelengths involved in OCT, electronic detection of backscattered light is not possible. Instead, optical interferometry is used to measure backreflections from tissue samples. Within the OCT interferometer, a broadband near infrared source (1310-nm center wavelength, 100-nm spectral bandwidth) is split into a reference and a sample field. The sample field is focused through the scanning optics to probe tissue at a depth corresponding to the optical pathlength of reference arm in the interferometer. The backscattered sample field mixes with the reference field returning from the reference mirror and a photodetector converts the interference fringe pattern into an electrical current. The amplitude of the interference fringe carries information about tissue structure and optical properties at the scanning depth defined by the reference arm. Tissue structure in a cross-section can be systematically probed in the depth or axial direction by varying the optical pathlength of the reference arm and in the lateral direction by rotating the sample beam circumferentially in the case of intravascular OCT. The electrical fringe signal is filtered, demodulated, digitized, and scan converted to form an OCT image.

Excised coronary arteries were collected from autopsies and stored in PBS at 4°C until imaging occurred, within 72 h. The OCT catheter had a diameter of 1.0 mm and, through rotation and longitudinal displacement (pullback) of the internal components, provided cross-sectional images of the entire length of the vessel segments. The catheter pullback rate was 0.5 mm/s, and the frame rate of the OCT system was 4 Hz (500 angular pixels  $\times$  250 radial pixels). The axial resolution was 10  $\mu\text{m}$  and the transverse resolution was 25  $\mu\text{m}$ . A visible light beam coincident with the infrared imaging beam was used to determine the longitudinal location of the imaging site. Ink marks were placed at imaging sites of interest for longitudinal registration with histology. In addition, a narrow diameter thread was placed between the catheter sheath and the lumen. An ink mark was applied to the vessel to denote the thread location in histology. Visualization of the thread on OCT and the ink mark in histology permitted rotational orientation of the two data sets. An example OCT image of a lipid rich plaque is shown in Fig. 1(A).

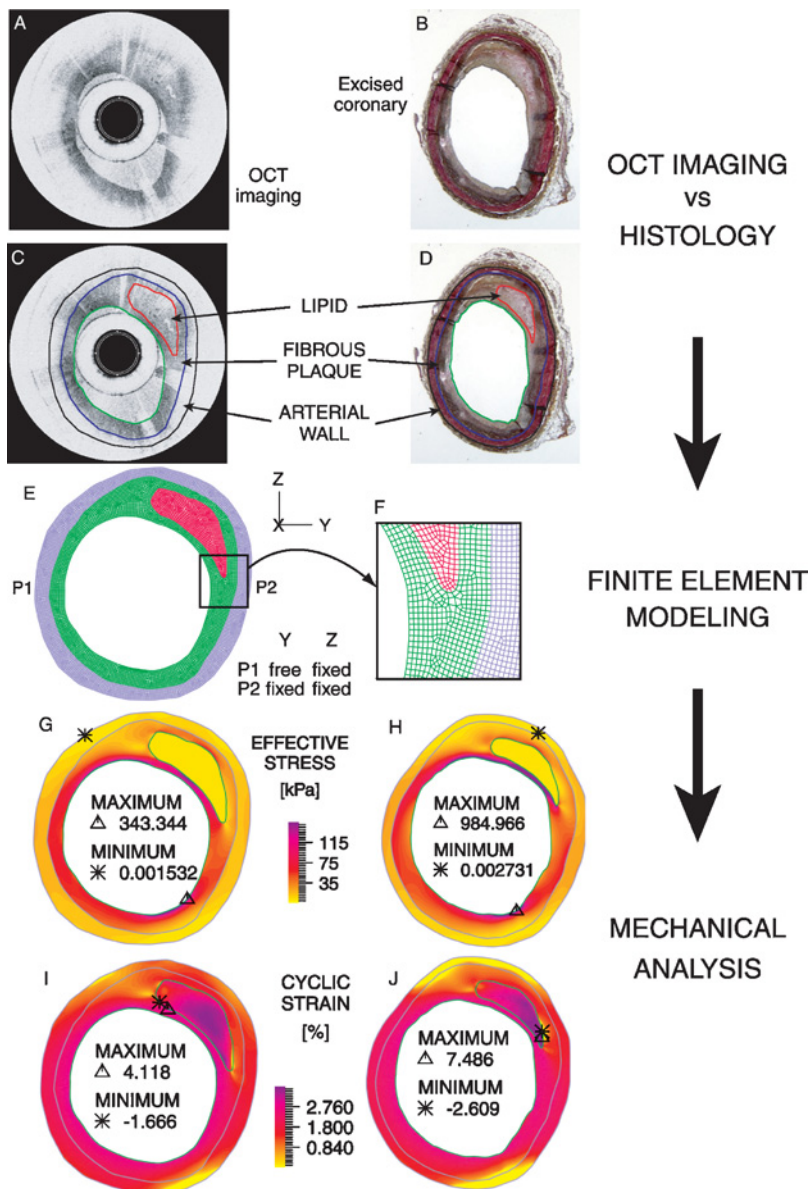


**FIGURE 1.** Finite element modeling process for a lipid rich coronary plaque cross-section. The OCT image (A) and histology image (B) are segmented (C,D) into lipid rich, fibrous plaque, and arterial wall regions. Each segmented image is used to create a finite element mesh (OCT mesh, E, with closeup in F). Application of an internal pressure load results in elevated stress at systolic pressure (G,H) and cyclic strain (I,J) distributions. Results for the OCT-based model are shown in the left column; results for the histology based model are shown in the right column.

#### *Histology Processing and Registration*

After imaging, the vessels were fixed in formalin and cut into segments for histology processing. Arteries with significant calcium content were decalcified as necessary. The vessels were embedded in paraffin and sliced into 4- $\mu$ m sections for staining with hematoxylin and eosin (H&E) or Movat's pentachrome. Histology slides were registered first with the ink marks made during imaging. Fine registration was accomplished using morphologic landmarks in the vessel wall such as calcium crystals and nod-

ules, eccentric stenoses, and lipid rich cores [Fig. 1(A) and 1(B)].

#### *Segmentation*

Histology segmentation (Fig. 1D) was performed by a vascular pathologist. OCT segmentation was performed by expert OCT readers who were blinded to the results from histology (Fig. 1C). Criteria for characterizing tissue types by OCT have been established previously.<sup>36</sup> Fibrous plaque is identified by homogeneous signal rich regions.

Lipid rich plaques are characterized by signal poor regions with diffuse borders, and calcific plaques exhibit signal poor regions with distinct borders. As the infrared OCT beam propagates through the lumen and into the tissue, it experiences attenuation through scattering and absorption. In heavily diseased arterial segments where the vessel wall thickness has significantly increased, attenuation can limit the ability of OCT to characterize deep structures near the adventitial surface of the vessels. In these cases, accurate segmentation of the full arterial cross-section can be challenging. Three OCT readers independently determined segmentations and the discrepancy between the results was used as a basis for assessing the impact of attenuation on mechanical modeling.

### Finite Element Analysis

Vessel contours from segmentation were imported into ADINA (Watertown, MA), a commercial finite element software package. A structured finite element mesh was created using 2D plane strain elements. The element edge length was approximately 30  $\mu\text{m}$ , which, based on grid convergence studies, was sufficiently fine. Each segmented region was assigned uniform isotropic material properties. All regions were given rubberlike Mooney-Rivlin material properties,<sup>3,30</sup> as defined by the strain energy density function

$$W = D_1(e^{D_2(I_1-3)} - 1)$$

where  $W$  is the strain energy density,  $D_1$  and  $D_2$  are material constants, and  $I_1$  is the first invariant of the Cauchy-Green deformation tensor. The product  $D_1 \times D_2$  is proportional to the elastic modulus of the material, while  $D_2$  is related to the strain-stiffening behavior of the material. The actual values used were taken from previous literature<sup>14</sup> (Table 1) in which values for fibrous plaque and calcification were calculated from previously published uniaxial test data,<sup>24</sup> lipid properties were adapted from previously published lipid data,<sup>26</sup> and arterial wall properties were taken directly from a previous study.<sup>8</sup>

The boundary conditions consisted of a fixed node on the right side of the outer boundary of the vessel and a point 180 degrees away that is free to move in one direction only [Fig. 1, 1(E) and 1(F)]. A pressure load was applied to the lumen of the vessel in 24 steps over the range of 0–16 kPa (0–120 mmHg).

**TABLE 1. Material properties.**

Material	$D_1$ [Pa]	$D_2$
Fibrous plaque	5105.3	13
Arterial Wall	2644.7	8.365
Lipid	50	5
Calcium	18,804.5	20

## RESULTS

The results of two example cases are presented. The first case is that of a lipid rich plaque (Fig. 1). Note that even though the OCT and histology images exhibit a close correspondence, they do not have identical geometry. In the OCT image, the lumen boundary is smooth with no jagged edges, but in the histology geometry there are many sharp edges in the lumen, particularly between the 5 and 6 o'clock position and the 10 and 11 o'clock position. Not coincidentally, this is also where the thin tissue section has folded upon itself during histology processing, as evidenced by the dark radial bands through the vessel wall at those locations (and to a lesser extent at the 3 and 9 o'clock positions). The folding may also explain why the artery appears to be more ellipsoid in histology than in OCT.

The finite element meshes [Fig. 1(E) and 1(F)] were inflated to systolic pressure and the resulting effective stress was examined [Fig. 1(G) and 1(H)]. The two stress distributions are qualitatively similar, with corresponding regions of high and low stresses. As expected, the lipid pool exhibits low stresses because it is a very compliant material and thus cannot carry much load. Being the stiffest material, the fibrous plaque carries most of the pressure load and therefore has higher stresses than the arterial wall and the lipid. High stresses are found in the fibrous cap covering the lipid pool, because the thin cap has to carry the share of the load that the lipid cannot support. High stresses are also found near the 5 o'clock position due to the curvature of the region. In both cases, this is the most kinked region of the lumen, naturally leading to focal stress concentrations. Although the maximum stress in the histology-based model is higher than in the OCT case (985 vs. 343 kPa), its location corresponds to a portion of the lumen that was folded in histology. This geometry artifact causes an erroneously high focal stress concentration in the histology-based model. If these artifactual maximum stress magnitudes are not considered, the stress distributions are similar between the OCT and histology models, a fact which is more easily appreciated by examining the stress distribution on a sector by sector basis. Each model was divided into 50 angular sectors centered at the centroid of the lumen. The mean stress, as well as the 25th and 75th percentiles of stress were calculated for each sector and plotted, along with the “unwrapped” geometry, as a function of angle [Fig. 2(B)]. The mean stresses, as well as the spread, are indeed similar throughout the cross section.

Cyclic strain, the difference in maximum principal strain between systolic and diastolic pressures (120 and 80 mm Hg), was also examined [Fig. 1(I) and 1(J)]. Again the overall strain distribution is qualitatively similar for both models with higher strains occurring in the lipid pool because it is compliant and displaces easily. Regions of the lipid pool border with the greatest curvature are expected to correspond to locations of highest strain. In this example,

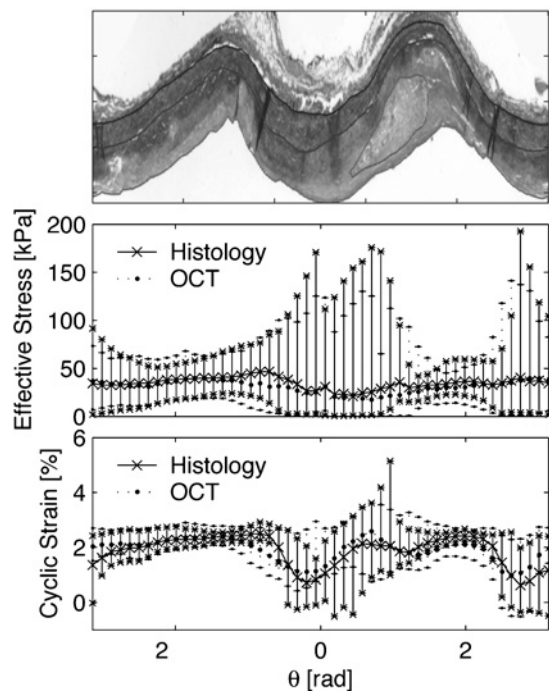


**FIGURE 2.** Lipid rich plaque histology, effective stress, and cyclic strain as a function of angle. (A) The “unwrapped” histology image. (B) Mean effective stress. (C) Mean cyclic strain. Mean values for histology-based model are plotted with x’s, OCT-based values are denoted with solid circles. Errorbars indicate the 25th and 75th percentile.

the histology-based model depicts a lipid pool having a border with significantly higher curvature than in the OCT model. The strain at this location was found to be 100% higher in the histology case compared with the OCT case. Despite these differences, the overall strain distributions are similar [Fig. 2(C)].

The second example is that of a calcified plaque (Fig. 3). The calcified region appears in the third quadrant. In the histology image, there is a small fold in the tissue at the 2 and 5 o’clock positions, and the tissue has undergone some tearing and separation of layers.

Typically, portions of the vessel cross-section with greater thickness should exhibit lower peak stress due to a distribution of the applied pressure load over a greater area. Correspondingly, high stresses in the calcified plaque model [Fig. 4(A) and 4(B)] are observed at the regions where the model vessel wall is thinnest overall—from 12 to 5 o’clock. Within the thin walled region, there are focal stress concentrations at the sharp corners of the mesh at 12, 1, and 5 o’clock in the histology model, and at 12 and 5 o’clock in the OCT model. Another curvature based stress concentration occurs at 10 o’clock. While the maximum stress in the histology based model is nearly 300% greater than that of OCT based model, the overall similarity of the stress distribution as a function of angle [Fig. 5(B)] suggests that these maxima are simply outliers.

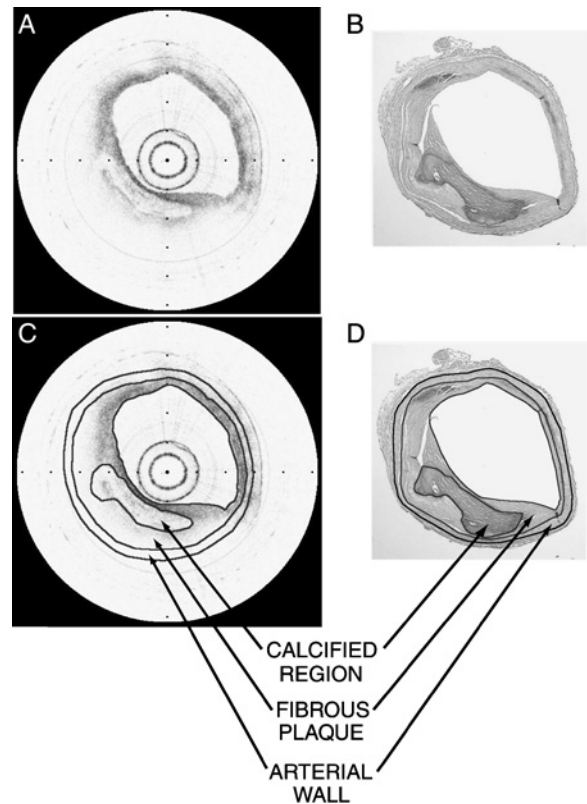


**FIGURE 3.** OCT image of a calcified plaque cross-section (A), and the corresponding histology section (B). Segmented OCT image (C), and segmented histology section (D).

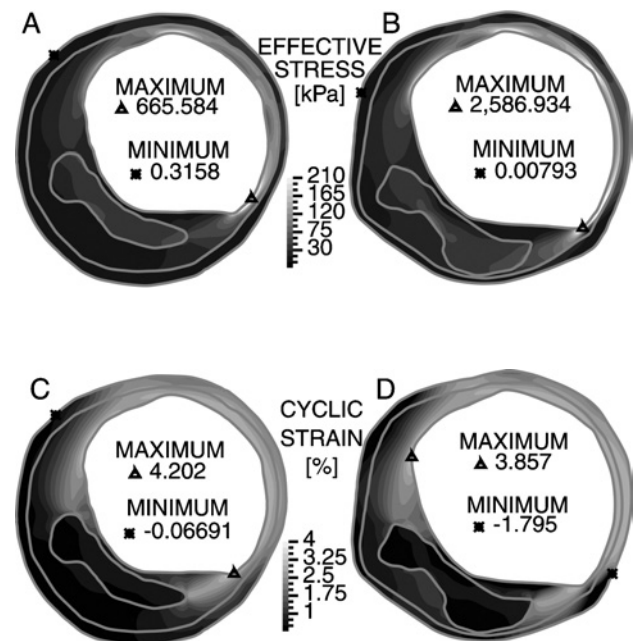


**FIGURE 4.** Calcified plaque effective stress, and cyclic strain. The left column shows results for the OCT-based finite element model, while the right column shows results for the histology-based model. Panels (A) and (B) depict stress at systolic pressure. Panels (C) and (D) depict cyclic strain.

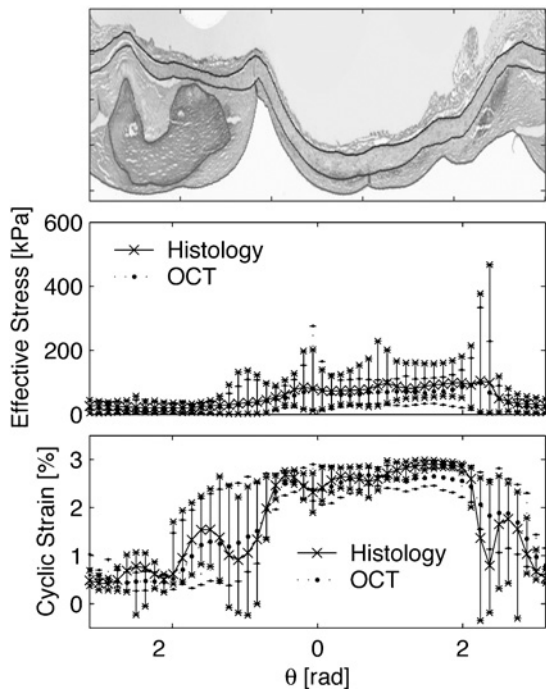


**FIGURE 5.** Calcified plaque histology, effective stress, and cyclic strain as a function of angle. (A) The “unwrapped” histology image. (B) Mean effective stress. (C) Mean cyclic strain. Error bars indicate the 25th and 75th percentile.

Elevated cyclic strain levels [Fig. 4(E) and 4(F)] occur again in the thinnest part of the artery. Because it is so stiff, the calcified region exhibits very little strain. Additionally, the part of the artery that lies beyond the calcified region is “shielded” from the load by the calcium nodule, and thus also sees little strain. Strain distributions between the two models are similar [Fig. 5(C)].

#### Sensitivity Analysis

The finite depth of penetration of OCT imaging poses a potential limitation for accurate modeling of vessel biomechanical properties. As the infrared OCT beam propagates into the tissue from the lumen, it experiences attenuation. Although the depth of penetration is sufficient to visualize the entire cross-section of normal human coronaries, it is frequently difficult to identify the adventitial structure in heavily diseased vessels. To investigate the potential impact of ambiguous segmentation on the modeling of biomechanical properties, a segmentation sensitivity analysis was performed. Each OCT image was given to two trained, nonpathologist OCT readers, and the resulting segmentation lines were used to create new finite element meshes.

For the lipid rich case, the alternate OCT readers found the plaque boundary to have a slightly different shape, and they were unable to determine an outer boundary for the

arterial wall. Thus one new model was created using the alternate plaque boundary, keeping all other boundaries the same [Fig. 6(A)]. A second model was created where the outer arterial wall boundary was taken to be a constant offset version of the plaque boundary [Fig. 6(C)].

The stress fields [Fig. 6(D), 6(E), and 6(F)] are remarkably similar in distribution and magnitude. The maximum stress of the alternate plaque model is 1% less than the original OCT based model, while the maximum stress of the constant offset outer boundary model is only 2% higher than that of the original OCT based model. The strain fields [Fig. 6(G), 6(H), and 6(I)] are similar as well, with the maximum strain differing by +0.5% and -1% for the alternate plaque and outer boundary models, respectively. One difference in the strain distribution can be seen within the lipid pool. The alternate plaque boundary model does not have a region of elevated strain in the center of the lipid pool as the other two models do. This reduced strain is expected, as the increased wall thickness results in greater stiffness overall.

The same sensitivity analysis was performed for the calcified plaque. In this case, the alternate OCT readers found the calcified region to be smaller than the pathologist had indicated. They also indicated the fibrous plaque region as smaller, and they were unable to completely determine the outer arterial wall boundary. A new model was constructed using alternate calcium nodule and fibrous plaque boundaries as drawn by the OCT readers [Fig. 7(B)]. The alternate arterial wall boundary was chosen to be a constant offset of the fibrous plaque boundary, with the offset distance approximated from the wall thickness measured in the first quadrant of the image.

Despite the significant change in model geometry, the overall stress distribution [Fig. 7(B) and 7(C)] does not change drastically in regions of interest. Regions of elevated and low stress still correspond and the locations of stress concentrations remain the same. The maximum stress differs by 10% and the maximum strain differs by 9%. The cyclic strain distributions [Fig. 7(E) and 7(F)] also exhibit modest differences. These results are not surprising despite the different shape of the calcified region and the decreased thickness of the arterial wall beyond. The calcified region is very stiff and thus has a “shielding” effect on the material around and behind it.

## DISCUSSION

In this study we have demonstrated the first use of OCT for finite element analysis. OCT based modeling and the accepted histology based modeling methods provide similar stress and strain distributions, but can yield disparate stress and strain magnitudes. These higher focal stress concentrations can arise from artificial sharp edges in the histology images that arise from nonuniform warping and folding of the tissue during histology processing.

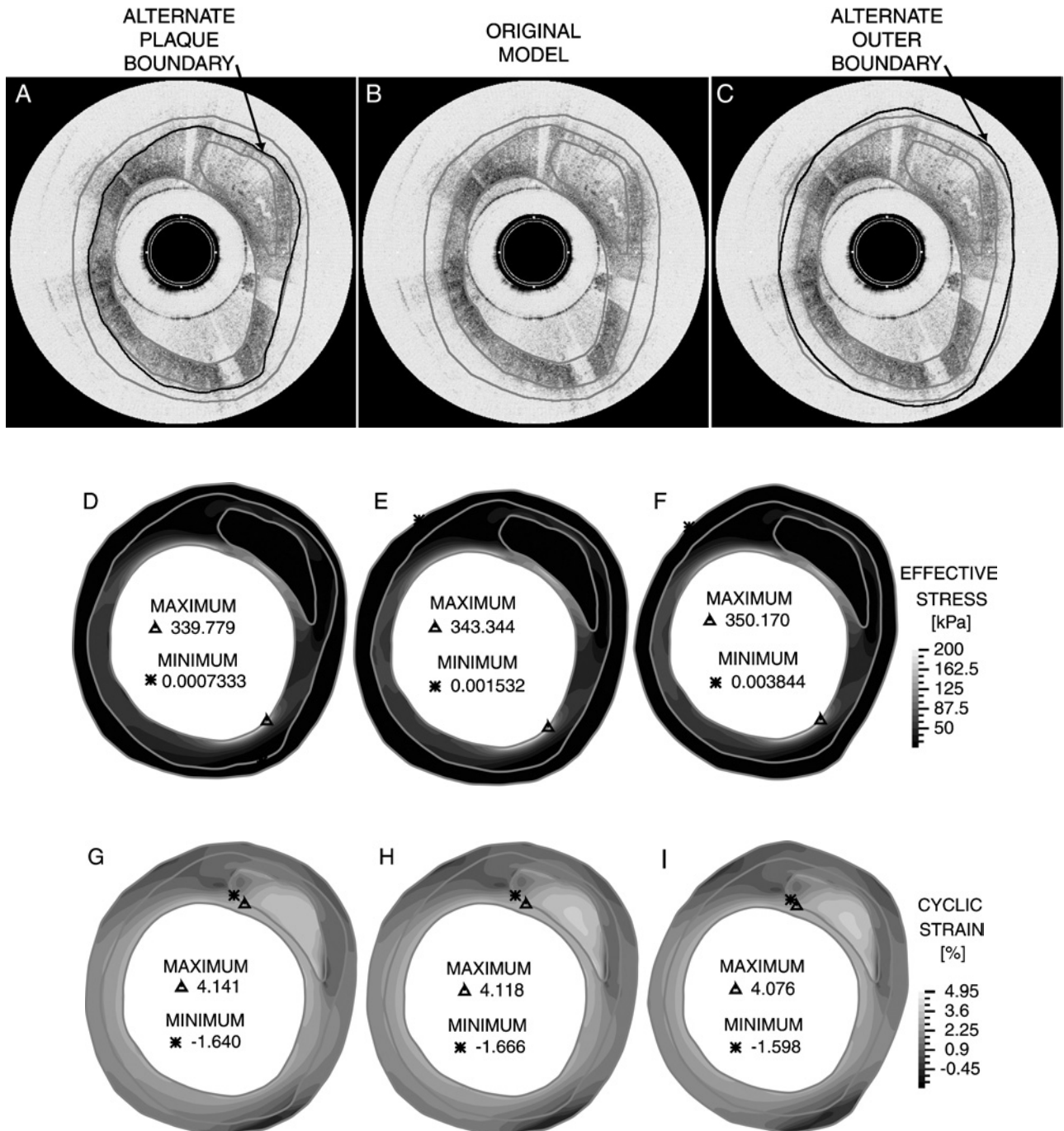


**FIGURE 6.** Segmentation sensitivity for the lipid-rich plaque. The left most column depicts an alternate plaque boundary model (dark line in the segmented OCT image), the center column depicts the original model, and the right column depicts a constant offset outer boundary model (dark line in the segmented OCT image). Panels (A), (B), and (C) are segmented OCT images, and panels (D), (E), and (F) show the corresponding stress fields, while panels (G), (H), and (I) present the resulting cyclic strain distributions.

Despite ambiguities in the segmentation of adventitial structure due to OCT signal attenuation, the resulting discrepancy in predicted cyclic strain was found to be modest for the vessel sections examined in this study. Much of the stress variation and the maximum values of stress and

strain tend to occur near the inner lumen of the vessel and are therefore only slightly influenced by changes in outer geometry. This is most striking in the case of calcified plaque. Since calcium has a relatively high stiffness, it has a stabilizing effect on the surrounding tissue<sup>14</sup> and

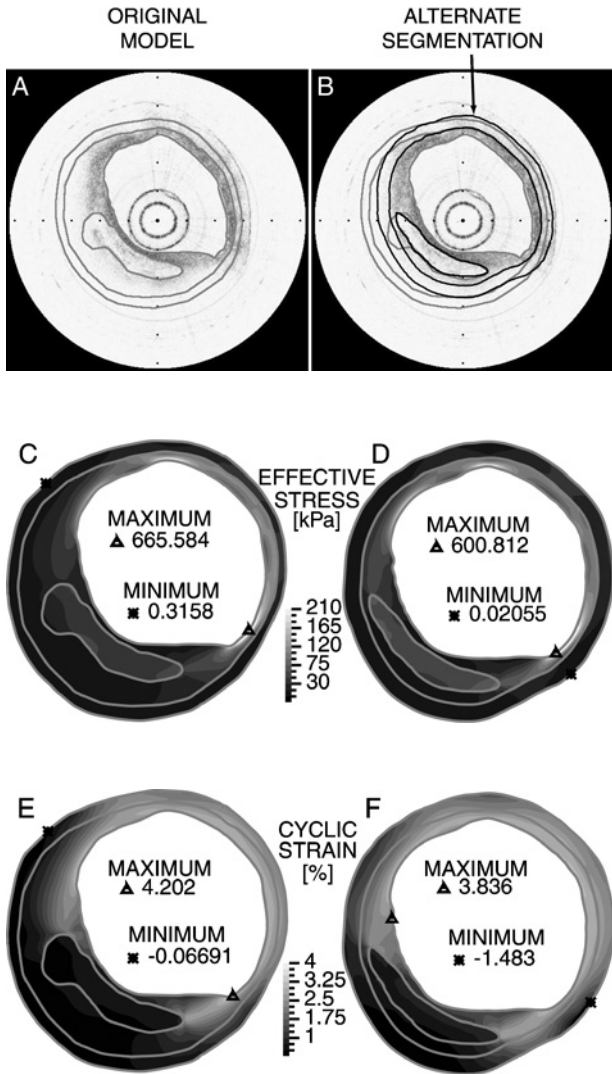


**FIGURE 7.** Segmentation sensitivity analysis for the calcified plaque. The left column depicts the original model, while the right column depicts the alternate segmentation model. In panel (B), the light lines show the original OCT model, while dark lines show the new segmentation lines. Panels (A) and (B) are segmented OCT images, (C) and (D) show the corresponding effective stress fields, and panels (E) and (F) present the resulting cyclic strain distributions.

acts to shield the adventitial regions from much of the mechanical load. It is also important to note that most acute myocardial infarctions are the result of an intimal disruption of a thin-capped, lipid rich plaque. Assessing the strain distribution near the lumen is therefore the most relevant goal for identifying and investigating vulnerable plaque.

The validity of finite element analysis in general is limited by the accuracy of the specific material model. Biological tissues are anisotropic and exhibit strain-stiffening behavior. Strain stiffening was incorporated into the analysis by using the Mooney-Rivlin material model, but anisotropy

was not accounted for in this study and should be included in future similar studies. Another limitation of the modeling applied in this study is that each tissue component was assigned a single modulus value. Although a more accurate model would address the natural heterogeneity of biological tissues, the measurement of modulus values for specific tissue types is challenging on even a macroscopic level and there is significant variation in the values assigned to vascular tissue in the literature. A recent study, however, has shown that stress fields are remarkably robust to variations in elastic modulus.<sup>35</sup>

Another limitation of this study is that the potential effect of residual stress was not considered. When an excised arterial segment is cut, it springs open, suggesting that in the uncut configuration, the artery is not in a stress-free state. Due to the lack of an accurate model to quantify the residual stress in an artery,<sup>15</sup> it is difficult to assess the impact of residual stress on resulting stress and strain fields. Nevertheless, studies have shown that the inclusion of residual stress tends to decrease the absolute magnitude of the resulting stresses and makes the stress and strain distributions more uniform.<sup>9,28</sup> A recent study found that the cyclic strain distribution remains relatively unchanged by the inclusion of residual stress.<sup>17</sup> In this study, the omission of residual stress should not affect the comparison of OCT and histology based finite element modeling.

Similar to most previous studies of vascular biomechanics, these results are based on two-dimensional analyses using the plane strain assumption. This assumption is valid if the vessel is either constrained longitudinally or if the longitudinal dimension is sufficiently large so that longitudinal strains are negligible. This may not be the case *in vivo*, as some segments of coronary vessels can undergo extension and high curvature during the cardiac cycle. Longitudinal variations in plaque geometry might also significantly alter stress and strain fields. OCT based finite element analysis is particularly attractive since, through longitudinal pull-back of the catheter during imaging, 3D images can be readily obtained. A similar 3D reconstruction based on histology slides would require a large number of histology slides, and would thus be prohibitively expensive and time consuming.

The purpose of this paper was to demonstrate the utility of using OCT images for finite element analysis of atherosclerotic plaques. This study can be extended by imaging the excised vessels undergoing inflation. The OCT- and histology-based finite element analyses can then be evaluated by comparing how well each analysis predicts the final arterial shape at a given pressure. Furthermore, finite element modeling of vessels inflated either *in vivo* or through an *ex vivo* experimental setup can be used to estimate patient-specific elastic modulus if the mechanical load and resulting deformation is known. Elastography is a method of strain imaging where sequential images of a tissue being deformed are used to estimate the strains in

the tissue.<sup>27</sup> Thus an iterative reconstruction method can be used with OCT elastography<sup>31</sup> to estimate the elastic modulus of real tissue.<sup>10,19</sup>

## CONCLUSION

Finite element analysis of coronary vasculature is a useful method to gain understanding of the biomechanical factors relevant to atherosclerosis. This paper presents the first use of OCT, an intravascular optical imaging modality, as a basis for finite element analysis. Comparison with the traditional histology based method shows that OCT based models exhibit similar stress and strain distributions. The results of a segmentation sensitivity analysis show that the stress and strain predictions are not significantly affected by segmentation ambiguities associated with OCT signal attenuation. Since OCT can be performed *in vivo* and at multiple time points, our results suggest that OCT-based finite element analysis may be a powerful tool for investigating coronary atherosclerosis, detecting vulnerable plaque, and monitoring response to therapy in living subjects.

## ACKNOWLEDGMENTS

The authors wish to acknowledge fruitful discussions with R. T. Lee. This study was funded by the National Institutes of Health (grant 5-R01-HL70039), and in part by the Center for Integration of Medicine and Innovative Technology (Cambridge, MA), and through a generous gift from Dr. and Mrs. J.S. Chen to the optical diagnostics program of the MGH Wellman Laboratories of Photomedicine.

## REFERENCES

- <sup>1</sup>American Heart Association. Heart and Stroke Facts: 1996. Statistical Supplement, Dallas, Texas.
- <sup>2</sup>American Heart Association. Heart Disease and Stroke Statistics: 2003. Update, Dallas, Texas.
- <sup>3</sup>Bathe, K.-J. Finite Element Procedures. Upper Saddle River, NJ: Prentice-Hall, 1996, pp. 592–594.
- <sup>4</sup>Becker, C. R., A. Knez, A. Leber, H. Treede, B. Ohnesorge, U. J. Schoepf, and M. F. Reiser. Detection of coronary artery stenoses with multislice helical CT angiography. *J. Comput. Assist. Tomogr.* 26:750–755, 2002.
- <sup>5</sup>Botnar, R. M., M. Stuber, K. V. Kissinger, W. Y. Kim, E. Spuentrup, and W. J. Manning. Noninvasive coronary vessel wall and plaque imaging with magnetic resonance imaging. *Circulation* 102:2582–2587, 2002.
- <sup>6</sup>Cheng, G. C., H. M. Loree, R. D. Kamm, M. C. Fishbein, and R. T. Lee. Distribution of circumferential stress in ruptured and stable atherosclerotic lesions—a structural-analysis with histopathological correlation. *Circulation* 87:1179–1187, 1993.
- <sup>7</sup>Davies, M. J. Stability and instability: Two faces of coronary atherosclerosis—the Paul Dudley White lecture 1995. *Circulation* 94:2013–2020, 1996.
- <sup>8</sup>Delfino, A. Analysis of stress field in a model of the human carotid. In: Physics. Lausanne: Ecole Polytechnique Federale De Lausanne, Lausanne, Switzerland, 1996.
- <sup>9</sup>Delfino, A., N. Stergiopoulos, J. E. Moore, and J. J. Meister. Residual strain effects on the stress field in a thick wall finite element model of the human carotid bifurcation. *J. Biomech.* 30:777–786, 1997.
- <sup>10</sup>Doyle, M. M., P. M. Meaney, and J. C. Bamber. Evaluation of an iterative reconstruction method for quantitative elastography. *Phys. Med. Biol.* 45:1521–1540, 2000.
- <sup>11</sup>Falk, E. Why do plaques rupture. *Circulation* 86:30–42, 1992.
- <sup>12</sup>Glagov, S., H. S. Bassiouny, Y. Sakaguchi, C. A. Goudet, and R. P. Vito. Mechanical determinants of plaque modeling, remodeling and disruption. *Atherosclerosis* 131 Suppl:S13–14, 1997.
- <sup>13</sup>Huang, D., E. A. Swanson, C. P. Lin, J. S. Schuman, W. G. Stinson, W. Chang, M. R. Hee, T. Flotte, K. Gregory, C. A. Puliafito, and J. G. Fujimoto. Optical coherence tomography. *Science* 254:1178–1181, 1991.
- <sup>14</sup>Huang, H., R. Virmani, H. Younis, A. P. Burke, R. D. Kamm, and R. T. Lee. The impact of calcification on the biomechanical stability of atherosclerotic plaques. *Circulation* 103:1051–1056, 2001.
- <sup>15</sup>Humphrey, J. D., and S. Na. Elastodynamics and arterial wall stress. *Ann. Biomed. Eng.* 30:509–523, 2002.
- <sup>16</sup>Jang, I. K., B. E. Bouma, D. H. Kang, S. J. Park, S. W. Park, K. B. Seung, K. B. Choi, M. Shishkov, K. Schlendorf, E. Pomerantsev, S. L. Houser, H. T. Aretz, and G. J. Tearney. Visualization of coronary atherosclerotic plaques in patients using optical coherence tomography: Comparison with intravascular ultrasound. *J. Am. Coll. Cardiol.* 39:604–609, 2002.
- <sup>17</sup>Kaazempur-Mofrad, M. R., H. F. Younis, S. Patel, A. Isasi, C. Chung, R. C. Chan, D. P. Hinton, R. T. Lee, and R. D. Kamm. Cyclic strain in human carotid bifurcation and its potential correlation to atherogenesis: Idealized and anatomically-realistic models. *J. Eng. Math.* 47:299–314, 2003.
- <sup>18</sup>Keeney, S., and P. Richardson. Stress analysis of atherosclerotic arteries. *IEEE Eng. Med. Biol.* 9:1484–1485, 1987.
- <sup>19</sup>Khalil, A., R. D. Kamm, B. E. Bouma, and M. R. Kaazempur-Mofrad. A genetic/FEM algorithm for parameter estimation: Application in characterization of atherosclerotic plaques. *J. Comput. Phys.*, Submitted.
- <sup>20</sup>Kolodgie, F. D., A. P. Burke, A. Farb, H. K. Gold, J. Y. Yuan, J. Narula, A. V. Finn, and R. Virmani. The thin-cap fibroatheroma: A type of vulnerable plaque—the major precursor lesion to acute coronary syndromes. *Curr. Opin. Cardiol.* 16:285–292, 2001.
- <sup>21</sup>Lee, R. T., A. J. Grodzinsky, E. H. Frank, R. D. Kamm, and F. J. Schoen. Structure-dependent dynamic mechanical-behavior of fibrous caps from human atherosclerotic plaques. *Circulation* 83:1764–1770, 1991.
- <sup>22</sup>Lee, R. T., H. M. Loree, G. C. Cheng, E. H. Lieberman, N. Jaramillo, and F. J. Schoen. Computational structural analysis based on intravascular ultrasound imaging before *in vitro* angioplasty: Prediction of plaque fracture locations. *J. Am. Coll. Cardiol.* 21:777–782, 1993.
- <sup>23</sup>Lee, R. T., H. M. Loree, and M. C. Fishbein. High stress regions in saphenous vein bypass graft atherosclerotic lesions. *J. Am. Coll. Cardiol.* 24:1639–1644, 1994.
- <sup>24</sup>Loree, H. M., A. J. Grodzinsky, S. Y. Park, L. J. Gibson, and R. T. Lee. Static circumferential tangential modulus of human atherosclerotic tissue. *J. Biomech.* 27:195–204, 1994.
- <sup>25</sup>Loree, H. M., R. D. Kamm, R. G. Stringfellow, and R. T. Lee. Effects of fibrous cap thickness on peak circumferential stress in model atherosclerotic vessels. *Circ. Res.* 71:850–858, 1992.

- <sup>26</sup>Loree, H. M., B. J. Tobias, L. J. Gibson, R. D. Kamm, D. M. Small, and R. T. Lee. Mechanical-properties of model atherosclerotic lesion lipid pools. *Arterioscler. Thromb.* 14:230–234, 1994.
- <sup>27</sup>Ophir, J., I. Cespedes, H. Ponnekanti, Y. Yazdi, and X. Li. Elastography: A quantitative method for imaging the elasticity of biological tissues. *Ultrason. Imaging* 13:111–134, 1991.
- <sup>28</sup>Patel, S. Y., M. R. Kaazempur-Mofrad, A. G. Isasi, and R. D. Kamm. Diseased artery wall mechanics: Correlation to histology. In: Proceedings of the 2003 Summer Bioengineering Conference, Key Biscayne, FL, June 25–29, 2003, pp. 499–500.
- <sup>29</sup>Richardson, P. D., M. J. Davies, and G. V. R. Born. Influence of plaque configuration and stress-distribution on fissuring of coronary atherosclerotic plaques. *Lancet* 2:941–944, 1989.
- <sup>30</sup>Rivlin, R. S. “Large elastic deformations of isotropic materials IV. Further developments of the general theory.” *Phil. Trans. R. Soc. Lond. A* 241:379–397, 1948.
- <sup>31</sup>Schmitt, J. M. Oct elastography: Imaging microscopic deformation and strain of tissue. *Opt. Express* 3:199–211, 1998.
- <sup>32</sup>Tearney, G. J., M. E. Brezinski, B. E. Bouma, S. A. Boppart, C. Pitris, J. F. Southern, and J. G. Fujimoto. In vivo endoscopic optical biopsy with optical coherence tomography. *Science* 276:2037–2039, 1997.
- <sup>33</sup>Tearney, G. J., I. K. Jang, and B. E. Bouma. Evidence of cholesterol crystals in atherosclerotic plaque by optical coherence tomography. *Eur. Heart J.* 24:1462, 2003.
- <sup>34</sup>Tearney, G. J., H. Yabushita, S. L. Houser, H. T. Aretz, I. K. Jang, K. H. Schlendorf, C. R. Kauffman, M. Shishkov, E. F. Halpern, and B. E. Bouma. Quantification of macrophage content in atherosclerotic plaques by optical coherence tomography. *Circulation* 107:113–119, 2003.
- <sup>35</sup>Williamson, S. D., Y. Lam, H. F. Younis, H. Huang, S. Patel, M. R. Kaazempur-Mofrad, and R. D. Kamm. On the sensitivity of wall stresses in diseased arteries to variable material properties. *J. Biomech. Eng. Trans. ASME* 125:147–155, 2003.
- <sup>36</sup>Yabushita, H., B. E. Bouma, S. L. Houser, T. Aretz, I. K. Jang, K. H. Schlendorf, C. R. Kauffman, M. Shishkov, D. H. Kang, E. F. Halpern, and G. J. Tearney. Characterization of human atherosclerosis by optical coherence tomography. *Circulation* 106:1640–1645, 2002.
- <sup>37</sup>Zaman, A. G., G. Helft, S. G. Worthley, and J. J. Badimon. The role of plaque rupture and thrombosis in coronary artery disease. *Atherosclerosis* 149:251–266, 2000.